

Article

# A Predictive Power Control Strategy for DFIGs Based on a Wind Energy Converter System

Xiaoliang Yang <sup>1,2</sup> , Guorong Liu <sup>1,3</sup>, Anping Li <sup>1</sup> and Van Dai Le <sup>4,5,\*</sup> 

<sup>1</sup> College of Electrical and Information Engineering, Hunan University, Changsha 410082, China; yangxl@hnu.edu.cn (X.Y.); lgr1110@126.com (G.L.); lianping@hnu.edu.cn (A.L.)

<sup>2</sup> College of Electrical and Information Engineering, Zhengzhou University of Light Industry, Zhengzhou 450002, China

<sup>3</sup> College of Electrical and Information Engineering, Hunan Institute of Engineering, Xiangtan 411100, China

<sup>4</sup> Institute of Research and Development, Duy Tan University, Da Nang 550000, Vietnam

<sup>5</sup> Faculty of Electrical Engineering, Industrial University of Ho Chi Minh City, Ho Chi Minh City 700000, Vietnam

\* Correspondence: levandai@iuh.edu.vn or levandai@duytan.edu.vn; Tel.: +84-901-672-689

Academic Editor: Marco Mussetta

Received: 7 June 2017; Accepted: 23 July 2017; Published: 26 July 2017

**Abstract:** A feasible control strategy is proposed to control a doubly fed induction generator based on the wind energy converter system (DFIG-WECS). The main aim is to enhance the steady state and dynamic performance under the condition of the parameter perturbations and external disturbances and to satisfy the stator power response of the system. Within the proposed control method, the control scheme for the rotor side converter (RSC) is developed on the model predictive control. Firstly, the self-adaptive reference trajectory is established from the deduced discrete state-space equation of the generator. Then, the rotor voltage is calculated by minimizing the global performance index under the current prediction steps at the sampling instant. Through the control scheme for the grid side converter (GSC) and wind turbine, we have re-applied the conventional control. The effectiveness of the proposed control strategy is verified via time domain simulation of a 150 kW-575 V DFIG-WECS using Matlab/Simulink. The simulation result shows that the control of the DFIG with the proposed control method can enhance the steady and dynamic response capability better than the conventional ones when the system faces errors due to the parameter perturbations, external disturbances and the rotor speed.

**Keywords:** doubly fed induction generator (DFIG); wind energy converter system (WECS); self-adaptive model predictive control; predictive power control

## 1. Introduction

### 1.1. Motivation

In previous years, there has been rapid growth in the renewable power generation industry, especially the wind power generation industry. It is reported that the global annual installed wind power capacity crossed the 60 million kilowatt (GW) mark in 2015 compared to 51.7 GW in 2014, and more than 63 GW of new wind power capacity was brought on line. Its market share and installed capacity continuously increase. Thanks to this, 2015 ranks as an unparalleled year for wind power generation industry as annual installations increased for the first time in history after a slowdown during the past few years [1]. According to the Global Wind Energy Council (GWEC), top markets in the world include PR China, USA, Germany, India, Spain, among which PR China and USA passed the 145 and 50 GW of wind energy installed mark by the end of 2015, respectively. With such a

penetration of large-scale wind power in the grid, more and more posed supposition should be considered to enhance the operating wind farms regarding the electrical system. Therefore, the wind energy conversion systems (WECS) should control and monitor to the best of their ability under various operating conditions of the electrical system when they are connected to the power grid.

During the last decades, several solutions for the renewable electricity generation have been exploited with the main aim of obtaining energy from wind speed under optimal conditions. Due to the wind speed variability, the most popular configuration for wind power generation is currently the doubly fed induction generator (DFIG) as shown in Figure 1. The WECS includes a wound rotor induction generator (WRIG) together with slip rings and a back-to-back voltage source converter (VSC), in which the WRIG’s rotor is connected to the grid through a back-to-back (BTB) converter, whereas the stator is directly connected to one, and this BTB is controlled by several schemes. In this way, DFIGs can operate over a range of speed between about 70% and 130% of the synchronous speed, so that they can carry up to 30% of the total power [2–4].

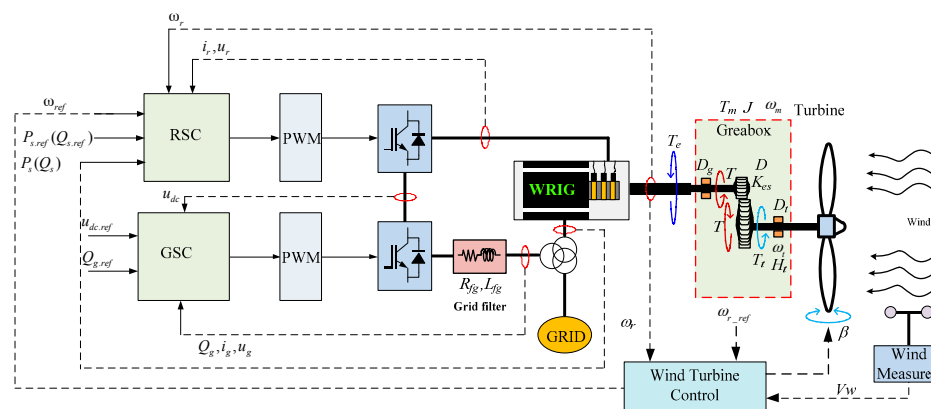


Figure 1. Schematic diagram of the DFIG-WECS.

In general, as shown in Figure 2, a variable-speed and-pitch DFIG-WECS has four operating zones, in which zones 2 and 3 are the most notable operating ones since the system operates in the variable-speed and -pitch modes, respectively. In a comparison with another wind turbine types, such as fixed-speed, variable-slip, and full-converter [5–7], DFIG has more advantageous characteristics. For example, it operates at optimal rotational speed for each given wind speed, reduces mechanical stresses, compensates for torque and power oscillations, and in particular, has the ability to control reactive power and decouple active and reactive power [8]. However, this system has a number of drawbacks, such as the limitation of the fault ride through capability, the inevitable need for slip rings, and more particularly in the complex control scheme for the converters to obtain the optimal generated power.

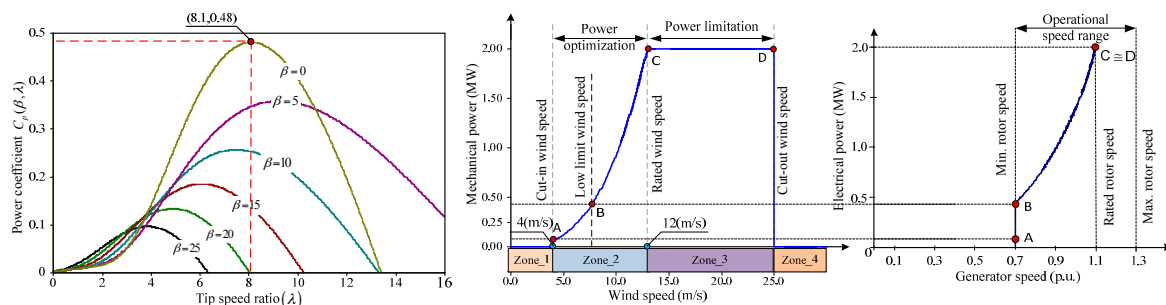


Figure 2. Ideal static curves for a DFIG-WECS.

## 1.2. State of the Science

Based on these facts, the control of a WSEC becomes more significant, especially when using the electrical generator based on DFIG. With many different purposes, the DFIG is controlled through many various control strategies. For example, vector control is used based on either a stator voltage oriented [9,10] or stator flux oriented [11–13] vector by using a  $d$ - $q$  synchronous frame for separately controlling the active and reactive power through a current controller. However, this method has the main disadvantage that depends highly on the parameters, such as the stator and rotor resistances and inductances. In order to overcome drawbacks from the vector method, in the mid-1980s, direct torque control (DTC) was examined in literature [14–16] to directly control the electromagnetic torque and the rotor flux of the DFIG by selecting the voltage vector from a predefined lookup table based on the stator flux and torque information. This control strategy has good characteristics, such as fast dynamic response, reliability, good perturbation rejection, and non-constant switching frequency behavior [5]. Nevertheless, its performance deteriorates during operation at low-speed. The predictive techniques [17], dither signal [18], and modified switching table [19] were proposed in order to solve this drawback. However, these strategies still have some disadvantages related to the hysteresis controllers that can cause the torque and current distortions and limit the steady-state accuracy [20]. Based on the same fundamentals of the DTC technique, direct power control (DPC) was proposed to independently and directly control the active and reactive power of DFIG based on the estimated reactive and active power and their errors. This control strategy has preponderant characteristics, such as fast dynamic response, grid disturbance, and robustness against parameter variations [21,22]. However, the performance of conventional DPC deteriorates due to the variable switching frequency. Moreover, the generated stator power can be controlled based on a portion of the turbine power by employing the feedback variable in the DPC controller [23]; the change in the turbine speed depends on the difference between turbine power and total generated power. Hence, this method can be degraded for controlling the generator speed and complicating the AC filter design. For improving the power control, the authors in [24,25] have proposed the scheme using the model-based predictive DPC technique.

For the purpose of excellent achievement of controlling the power for DFIG system under satisfactory stator power response, predictive control is an alternative control strategy. A new strategy based on the predictive direct power control (P-DPC) method is proposed in [26] to control the power at low constant switching frequency. The obtained results are satisfactory. However, the active and reactive power output is directly predicted. Authors in [27] introduced a direct power control method based on the finite model predictive control by using a discrete prediction model and a cost function to select the switching vector and to realize the optimal tracking control. In this way, the multi-objective optimization can easily be obtained by selecting different cost functions such that it does not have to use the coordinate transformation and the pulse wave modulation with a fast response [28]. However, this method still has drawbacks, such as the long calculation time of multi-step prediction, strong dependence on model parameters, and unfixed switching frequency. Besides, in order to realize the rapid power tracking, authors in [29] improved the predictive control for DC/AC converters based on DPC that was presented in [30]. Nevertheless, the calculated output reactive and active power and the time calculation still depend on the generator parameters and the compensative feedback of disturbance is not designed, and these are its main drawbacks.

Generally, the stator power and state-space equations of DFIG play an important role in directly controlling the stator active and reactive power. Based on such that, the author in [31] proposed a model predictive control method based on the state-space equations of stator power and rotor voltage to realize the power tracking control. Nonetheless, they failed to measure the error feedback and input limitation and to control the flexibly dynamic response. Having the same issue, the sliding-mode control method was introduced in [32,33] to perform tracking power control. The redemption of these methods is to establish the state-space equations of power and rotor voltage into the approximate

equations, so that the internal uncertainties and external disturbances are large in practical operation, resulting in the serious oscillations and the secure over-boundary of the system.

### 1.3. Contribution

To enhance the steady-state and transient control performance of DFIG-WCES for the purpose of satisfying the stator power output response according to given wishful values under the impact of the errors due to the parameter perturbations and external disturbances, in this context, the authors propose a relevant control scheme for the rotor-side converter (RSC). This proposed method is developed based on: Firstly, to establish a novel discrete state-space model of DFIG in the stator voltage oriented reference frame, considering the stator power and the rotor voltage as the state and control variables, respectively. Secondly, to propose the self-adaptive model predictive control scheme based on the model predictive control (MPC) using the discrete state-space model considering the impact of errors and performance index. Then, the stability condition of the obtained control signal for the closed-loop of the whole system is carried for analysis. For the grid side converter (GSC) and wind turbine control strategies, we have re-applied the conventional control strategy as proposed by authors in [34].

The remainder of the paper is organized as follows: in Section 2, we explain the mathematical model of WECS-DFIG including the wind turbine and generator. The methodology is introduced in Section 3 to establish the relevant control scheme for the RSC. The case studies and results are displayed in Section 4. Finally, the conclusions are given in Section 5, and the parameters of the controllers and studied system are listed in Appendix A.

## 2. Mathematical Model of the Wind Energy Converter System

Figure 1 illustrates a wind energy converter system based on the doubly fed induction generator (WECS-DFIG), including the wind turbine, the control systems, electric generator, connected to the grid.

### 2.1. Dynamic Model of the Wind Turbine

The presentation of the mechanical system of the whole wind turbine is complex. For the purpose of modeling and simulation, the two-mass drive train model is proposed to study the dynamic stability of the mechanical system. The electromechanical dynamics are presented by the following equations [35]:

$$J \frac{d\omega_m}{dt} = T_m - T_e - C_f \omega_m, \quad (1)$$

where  $J$  is the inertia of the generator-turbine system,  $T_e$  is the electromagnetic torque,  $C_f$  is the frictional coefficient,  $\omega_m$  is the rotor mechanical angular speed,  $P_m$  is the turbine mechanical power and is given as [36,37]:

$$P_m = P_w C_p(\beta, \lambda), \quad (2)$$

The wind power swept can be converted depending on the air density  $\rho$ , the turbine blade radius  $R$ , the wind speed  $V_w$ , as:

$$P_w = \frac{1}{2} \rho \pi R^2 V_w^3. \quad (3)$$

The power coefficient can be defined as:

$$C_p(\beta, \lambda) = \sum_{i=0}^4 \sum_{j=0}^4 \alpha_{ij} \beta^i \lambda^j. \quad (4)$$

The turbine tip-speed ratio  $\lambda$  is defined as:

$$\lambda = \frac{\omega_t R}{V_w}, \quad (5)$$

The factors  $\alpha_{i,j}$  are listed in Table 1 [36].

**Table 1.** The coefficients of  $\alpha_{ij}$  for  $i,j = 0, 1, \dots, 4$ .

$i/j$	0	1	2	3	4
0	$-4.1909 \times 10^{-1}$	$2.1808 \times 10^{-1}$	$-1.2406 \times 10^{-2}$	$-1.3365 \times 10^{-4}$	$1.1524 \times 10^{-5}$
1	$-6.7606 \times 10^{-2}$	$6.0405 \times 10^{-2}$	$-1.3934 \times 10^{-2}$	$1.0683 \times 10^{-3}$	$-2.3895 \times 10^{-5}$
2	$1.5727 \times 10^{-2}$	$-1.0996 \times 10^{-2}$	$2.1495 \times 10^{-3}$	$-1.4855 \times 10^{-4}$	$2.7937 \times 10^{-6}$
3	$-8.6018 \times 10^{-4}$	$5.7051 \times 10^{-4}$	$-1.0479 \times 10^{-4}$	$5.9924 \times 10^{-6}$	$-8.9194 \times 10^{-8}$
4	$1.4787 \times 10^{-5}$	$-9.4839 \times 10^{-6}$	$1.6167 \times 10^{-6}$	$-7.1535 \times 10^{-8}$	$4.9686 \times 10^{-10}$

The turbine output mechanical torque of WECS-DFIG can be derived as follows

$$T_m = \frac{P_m}{\omega_t}, \quad (6)$$

where  $\omega_t$  is the turbine rotational angular speed.

## 2.2. Generator Model

The generator is used for the objective of this study to be the wound rotor induction generator (WRIG); its expressions are written in the synchronous rotating  $d$ - $q$  reference frame and can be expressed as [5,34,38]:

The  $d$ - $q$  components of stator and rotor voltages are, respectively:

$$\begin{cases} u_{sd} = R_s i_{sd} + \frac{d\lambda_{sd}}{dt} - \omega_s \lambda_{sq} \\ u_{sq} = R_s i_{sq} + \frac{d\lambda_{sq}}{dt} + \omega_s \lambda_{sd} \\ u_{rd} = R_r i_{rd} + \frac{d\lambda_{rd}}{dt} - (\omega_s - \omega_r) \lambda_{rq} \\ u_{rq} = R_r i_{rq} + \frac{d\lambda_{rq}}{dt} + (\omega_s - \omega_r) \lambda_{rd} \end{cases} \quad (7)$$

The  $d$ - $q$  components of stator and rotor fluxes are, respectively:

$$\begin{cases} \lambda_{sd} = L_s i_{sd} + L_m i_{rd} \\ \lambda_{sq} = L_s i_{sq} + L_m i_{rq} \\ \lambda_{rd} = L_m i_{sd} + L_r i_{rd} \\ \lambda_{rq} = L_m i_{sq} + L_r i_{rq} \end{cases} \quad (8)$$

The stator active and reactive powers are, respectively:

$$\begin{cases} P_s = \frac{3}{2} (u_{sd} i_{sd} + u_{sq} i_{sq}) \\ Q_s = \frac{3}{2} (u_{sq} i_{sd} - u_{sd} i_{sq}) \end{cases} \quad (9)$$

where  $L_s$ ,  $L_r$  and  $L_m$  are the stator, rotor, and mutual inductances, respectively;  $R_s$  and  $R_r$  are the stator and rotor resistances, respectively;  $\omega_s$  the synchronous angular speed; and  $\omega_r$  is the angular frequency of the rotor calculated as  $p\omega_m$ , where  $p$  is number of pole pairs.

## 2.3. Modeling of Generator for Predictive Power Control

The WECS-DFIG power control guides the independent stator active and reactive powers by regulating the rotor flux. For this purpose, the stator active and reactive powers are represented as

functions of each individual rotor flux. We use the stator voltage vector oriented control ( $u_{sd} = u_s$  and  $u_{sq} = 0$ ) that decouples the  $dq$  axis. Thus, Equation (8) becomes

$$\begin{cases} i_{sd} = \frac{L_m}{L_m^2 - L_s L_r} \lambda_{rd} \\ i_{sq} = \frac{L_m}{L_m^2 - L_s L_r} \left( \lambda_{rq} + u_s \frac{L_r}{L_m \omega_s} \right), \end{cases} \quad (10)$$

The stator active and reactive powers can be calculated by substituting Equations (10) into (9); we have:

$$\begin{cases} P_s = -\frac{3}{2} u_s K_\sigma \lambda_{rd} \\ Q_s = \frac{3}{2} u_s K_\sigma \left( \lambda_{rq} + u_s \frac{L_r}{L_m \omega_s} \right), \end{cases} \quad (11)$$

where  $K_\sigma = L_m / \sigma L_s L_r$  is constant and  $\sigma = 1 - (L_m^2 / L_s L_r)$  is the leakage factor.

Equation (7) indicates that the rotor voltage directly controls rotor fluxes when neglecting the rotor resistance. In addition, as seen in Equation (11), the rotor fluxes will reflect on the stator active and reactive powers. Thus, this basis can be used in controlling the stator active and reactive power of the WECS-DFIG on its rotor side.

Taking the time derivative of Equation (11) along the trajectory of the rotor flux and combining Equation (7) under the stator voltage vector oriented control mode, neglecting the rotor resistance, the stator active and reactive power becomes:

$$\begin{aligned} \frac{d}{dt} \begin{bmatrix} P_s(t) \\ Q_s(t) \end{bmatrix} &= \begin{bmatrix} 0 & -(\omega_s - \omega_r) \\ (\omega_s - \omega_r) & 0 \end{bmatrix} \begin{bmatrix} P_s(t) \\ Q_s(t) \end{bmatrix} + \begin{bmatrix} -\frac{3}{2} u_s K_\sigma & 0 \\ 0 & \frac{3}{2} u_s K_\sigma \end{bmatrix} \begin{bmatrix} u_{rd}(t) \\ u_{rq}(t) \end{bmatrix} \\ &+ \begin{bmatrix} 1 & 0 \\ 0 & 1 \end{bmatrix} \begin{bmatrix} \frac{(\omega_s - \omega_r)}{\omega_s} \left( \frac{3}{2} u_s^2 K_\sigma \frac{L_r}{L_m} \right) \\ 0 \end{bmatrix}, \end{aligned} \quad (12)$$

Assume that the mechanical angular speed of the rotor is greater than that of the electricity [39], so that the mechanical angular speed is constant and is a valid approximation to each sample period [40,41]. Hereby, the slip speed is constant, due to the synchronous speed being clamped by the grid frequency.

Apply the zero order hold with no delay to discretize Equation (12) considering the sampling period  $T$  and the sampling time  $k$  [42]. In addition, due to the applied rotor side, the voltage is constant during a power control period for the pulse width modulation (PWM) converter. Therefore, Equation (12) becomes

$$\begin{aligned} \underbrace{\begin{bmatrix} P_s(k+1) \\ Q_s(k+1) \end{bmatrix}}_{x(k+1)} &= \underbrace{\begin{bmatrix} 1 & -(\omega_s - \omega_r)T \\ (\omega_s - \omega_r)T & 1 \end{bmatrix}}_A \underbrace{\begin{bmatrix} P_s(k) \\ Q_s(k) \end{bmatrix}}_{x(k)} + \underbrace{\begin{bmatrix} -\frac{3}{2} u_s K_\sigma T & 0 \\ 0 & \frac{3}{2} u_s K_\sigma T \end{bmatrix}}_B \underbrace{\begin{bmatrix} u_{rd}(k) \\ u_{rq}(k) \end{bmatrix}}_{u(k)} \\ &+ \underbrace{\begin{bmatrix} T & 0 \\ 0 & T \end{bmatrix}}_G \underbrace{\begin{bmatrix} \frac{(\omega_s - \omega_r)}{\omega_s} \left( \frac{3}{2} u_s^2 K_\sigma \frac{L_r}{L_m} \right) \\ 0 \end{bmatrix}}_{w(k)}. \end{aligned} \quad (13)$$

Equation (13) can be rewritten under the following space-state form

$$\begin{cases} x(k+1) = Ax(k) + Bu(k) + Gw(k), \\ y(k+1) = Cx(k+1), \end{cases} \quad (14)$$



disturbances; (ii) designing the self-adaptive reference trajectory on the model predictive method. Figure 4 illustrates the relationship between the input and output of the system model, and the procedure is performed as follows:

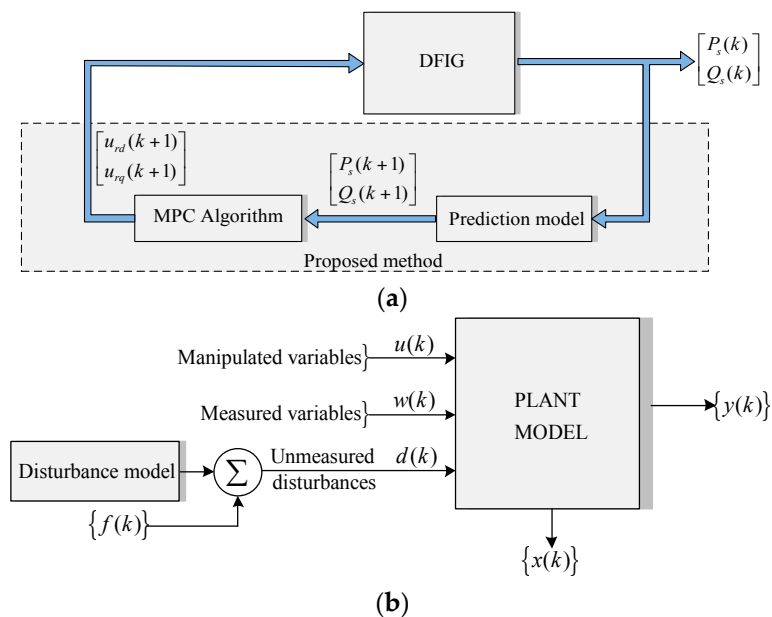


**Figure 4.** General concept of the proposed rotor side converter (RSC) control method: (a) General schematic; (b) Discrete-time system overview with disturbances.

### 3.1.1. Impact of Errors

Suppose that the model in Equation (14) is influenced by the parameter perturbation and external disturbances. The discrete-time predictive model can be obtained due to these errors as a state-space model as follows:

$$\begin{cases} x(k+1) = (A + \Delta A)x(k) + (B + \Delta B)u(k) + Gw(k) + f(k) \\ y(k+1) = Cx(k+1), \end{cases} \quad (16)$$

where  $\Delta A$  and  $\Delta B \in \mathbb{R}^{2 \times 2}$  are the parameter perturbations matrices and  $f(k)$  is the external disturbances vector.

The system in Equation (16) contains the state vector  $x(k)$ . Calculate the difference between this state vector  $x(k)$  and the desired state vector  $x^*(k)$ ; the error state-space model is generated under the condition of the error state-space functions  $e(k) = x(k) - x^*(k)$  and  $e(k+1) = x(k+1) - x^*(k+1)$ , and then  $e$  substitutes these error state-space functions into Equation (16). Therefore, the error state-space model can be obtained as follows:

$$\begin{cases} e(k+1) = Ae(k) + Bu(k) + \tilde{x}(k) + Gw(k) + d(k) \\ y_e(k+1) = C_e e(k+1), \end{cases} \quad (17)$$

where the corresponding components are:

$$\begin{cases} d(k) = \Delta Ax(k) + \Delta Bu(k) + f(k) \\ \tilde{x}(k) = Ax^*(k) - x^*(k+1). \end{cases} \quad (18)$$

Supposing that if the system in Equation (17) operates under the nominal condition, in other words  $d(k) = 0$ , the error state-space model becomes:

$$\begin{cases} e(k+1) = Ae(k) + Bu(k) + \tilde{x}(k) + Gw(k) \\ y_e(k+1) = C_e e(k+1), \end{cases} \quad (19)$$

where  $y_e(.) \in \mathbb{R}^2$  and  $C_e \in \mathbb{R}^{2 \times 2}$  are the output vector and matrix, respectively.

Therefore, the system in Equation (19) is used as the basis to design the RSC controller whose objective is to obtain the output vector  $y_e(k)$  equal to zero. In order to reach this objective, the output matrix  $C_e$  can be determined from the pole assignment according to the design method of sliding mode surface, which was described in [43].

### 3.1.2. Design Self-Adaptive Model Predictive Controller

The basic idea of a self-adaptive model predictive controller is to control the active and reactive power flow between the stator and grid according to a given value based on the model predictive control (MPC). As above-mentioned, the objective is to control the output vector  $y_e(k)$  of the state-space model in Equation (19) to reach zero. The procedure is done as follows:

#### Output Prediction

MPC is based on the predictions of future outputs over a prediction horizon having length  $P$  and the effect of changing the control horizon move  $M$ , as shown in Figure 5 [44]. In this study, we consider  $P \geq M$ . The current control horizon move  $M$  happens in the system at the current sampling instant  $k$  and the future control move is kept invariant. The predictions of the whole system (19) can be obtained as [45]:

$$y_P(k+P) = C_e A^P e(k) + \sum_{i=1}^P C_e A^{i-1} B u(k+P-i) + \sum_{i=1}^P C_e A^{i-1} \tilde{x}(k+P-i) + \sum_{i=1}^P C_e A^{i-1} G w(k+P-i). \quad (20)$$

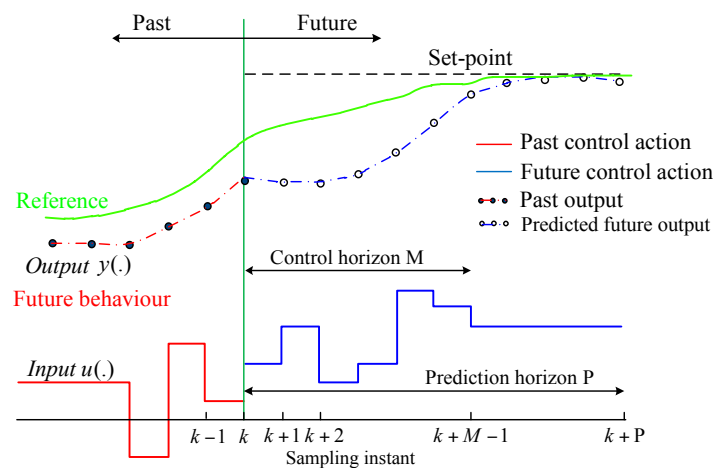


Figure 5. General concept for model predictive control (MPC).

The dimension of the  $P$  in Equation (20) plays an important role in improving controller performance. In this study, this value is set equal to 2 and the control horizon has a value of 1.

The output prediction state when having a control move from time  $(k - P)$  to time  $k$  can be obtained as [46]

$$y_y(k + P) = C_e A^P e(k - P) + \sum_{i=1}^P C_e A^{i-1} B u(k - i) + \sum_{i=1}^P C_e A^{i-1} \tilde{x}(k - i) + \sum_{i=1}^P C_e A^{i-1} G w(k - i), \quad (21)$$

We now consider the internal and external uncertain factors of the prediction model that results in the output at a future time of the system in Equation (20), so that the accuracy of the prediction is affected. The error between the current actual output  $y_e(k)$  of the error state-space model in Equation (19) at time  $k$  and the predictive output  $y_y(k + P)$  in Equation (21) is used as the feedback correction of the predicted output  $y_P(k + P)$ . Therefore, the predictive output of the closed-loop model can be obtained as follows [46]:

$$\hat{y}_P(k + P) = y_P(k + P) + H_P(y_e(k) - y_y(k + P)), \quad (22)$$

where  $H_P \in \mathbb{R}^{2P \times 2P}$  is the diagonal coefficient matrix used to adjust the proportion of the feedback errors. Applying engineering, the initial value of  $H_P$  is usually selected between 0 and 1 [46], and for this study, the first and second values are chosen:

$$H_1 = \begin{bmatrix} 0.9 & 0 \\ 0 & 0.9 \end{bmatrix}, H_2 = \begin{bmatrix} 0.45 & 0 \\ 0 & 0.45 \end{bmatrix}. \quad (23)$$

As known, the existing feedback correction mechanism could produce the tracking delay and overshoot under an input step and so, for the rapid dynamic response system, this feedback correction mechanism is removed to enhance the dynamic response performance, whereas, the anti-disturbance performance does not take notice during processing. Therefore, in order to solve this problem, in this study, we propose an appropriate control threshold for  $H_p$ , that is, the feedback correction mechanism is removed when  $\|e(k)\|_1 \geq 10^4$  and vice versa.

### Reference Trajectory

In MPC applications, the reference trajectory is one of the advantages of a predictive control scheme. The reference trajectory denotes a first order exponential curve used to make a gradual transition to the desired set-point value. If the value of the output function  $y(k)$  should move to the desired value  $r(k)$  along a reference trajectory with respect to the sampling time instant  $k$ , the output reference trajectory over the prediction horizon can be denoted as [46]:

$$\begin{aligned} y_r(k + P) &= \zeta y_r(k + P - 1) + (1 - \zeta)r(k + P) \\ y_r(k) &= y_e(k) \end{aligned} \quad (24)$$

where  $\zeta = \text{diag}\left\{\frac{\gamma + \tau\|e(k)\|_1}{\mu + \|e(k)\|_1}, \dots, \frac{\gamma + \tau\|e(k)\|_1}{\mu + \|e(k)\|_1}\right\}$  is an adjustable variable, in which  $0 < \gamma < \mu, 0 < \tau < 1$ , this value constitutes an adjustable value  $0 < (\gamma + \tau\|e(k)\|_1) / (\mu + \|e(k)\|_1) < 1$  that could influence the response of the system. Figure 6 plots two trajectory forms according to two different values of  $\zeta$  when the reference  $r(k + P)$  is constant. Observed from this figure, the reference trajectory is fast tracked according to the small values of  $\zeta$  as shown in the curve of  $y_{r,1}(k + P)$ ; if this value of  $\zeta$  is increased, the reference trajectory becomes the curve of  $y_{r,2}(k + P)$ , slowly giving rise to a smoother response.

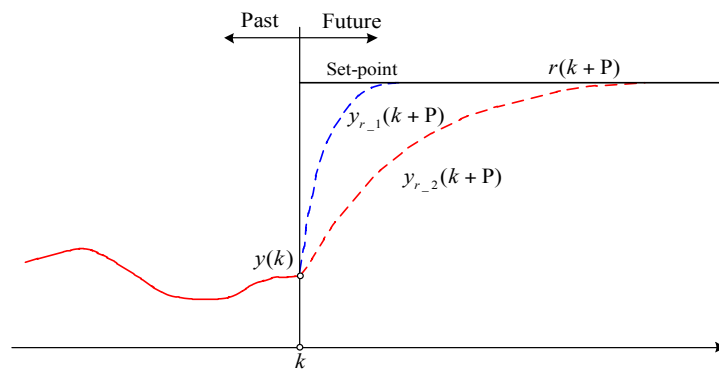


Figure 6. Reference trajectory according to the different values of  $\zeta$ .

### Performance Index

The MPC is one of the few control strategies having the ability to cope with the constrained system providing an optimal control for a certain performance index. The objective of the whole system is to regulate the system output to the wishful values while keeping the performance index minimal and satisfying the above constraints. We now consider an MPC design problem with the global optimization performance index of the whole system at the sampling time instant  $k$  as [45]:

$$J(k) = \sum_{i=1}^P \|y_r(k+i) - \hat{y}_P(k+i)\|_{Q_i}^2 + \sum_{j=1}^M \|u(k+j-1)\|_{R_j}^2, \tag{25}$$

where  $Q$  and  $R$  are the weighting matrices used to measure the importance degree of the tracking error and control variable in performance indexes.

The local performance index of the whole system can be rewritten under the matrix form using quadratic programming notation [47], that is:

$$J(k) = (Y_r(k+1) - \hat{Y}_P(k+1))^T Q (Y_r(k+1) - \hat{Y}_P(k+1)) + U(k)^T R U(k), \tag{26}$$

where the corresponding components are the follows:

$$\begin{cases} \hat{Y}_P(k+1) = [\hat{y}_P(k+1), \dots, \hat{y}_P(k+P)]^T \\ Y_r(k+1) = [y_r(k+1), \dots, y_r(k+P)]^T \\ U(k) = [u(k), \dots, u(k+M-1)]^T \\ Q = \text{diag}\{Q_1, \dots, Q_P\} \\ R = \text{diag}\{R_1, \dots, R_M\}. \end{cases} \tag{27}$$

Transforming Equations (20)–(22) and (24) into the state-space form and then substituting them into Equation (26), we have:

$$J(k) = \begin{pmatrix} Z y_e(k) - F e(k) - G U(k) - V \tilde{X}(k) - L W(k) - H E(k) \\ -G U(k) - V \tilde{X}(k) - L W(k) - H E(k) \end{pmatrix}^T Q \begin{pmatrix} Z y_e(k) - F e(k) \\ -G U(k) - V \tilde{X}(k) - L W(k) - H E(k) \end{pmatrix} + U(k)^T R U(k), \tag{28}$$

where

$$\left\{ \begin{array}{l} F = [C_e A, \dots, C_e A^P]^T, \\ G = \begin{bmatrix} C_e B & 0 & \dots & 0 \\ \vdots & \vdots & \vdots & \vdots \\ C_e A^{M-1} B & \dots & C_e B & \\ \vdots & \vdots & \vdots & \\ C_e A^{P-1} B & \dots & \sum_{i=1}^{P-M+1} C_e A^{i-1} B & \end{bmatrix}, \\ V = \begin{bmatrix} C_e & 0 & \dots & 0 \\ C_e A & C_e & \dots & 0 \\ \vdots & \vdots & \vdots & \vdots \\ C_e A^{P-1} & C_e A^{P-2} & \dots & C_e \end{bmatrix}, \end{array} \right. \quad \begin{array}{l} L = \begin{bmatrix} C_e G & 0 & \dots & 0 \\ C_e A G & C_e G & \dots & 0 \\ \vdots & \vdots & \vdots & \vdots \\ C_e A^{P-1} G & C_e A^{P-2} G & \dots & C_e G \end{bmatrix}, \\ H = \text{diag}\{H_1, \dots, H_P\}, \\ Z = [\zeta^1, \dots, \zeta^P]^T, \\ \tilde{X}(k) = [\tilde{x}(k), \dots, \tilde{x}(k+P-1)]^T, \\ W(k) = [w(k), \dots, w(k+P-1)]^T, \\ E(k) = [y_e(k) - y_y(k), \dots, y_e(k) - y_y(k+P)]^T, \\ U(k) = [u(k+1), \dots, u(k+M)]^T. \end{array} \quad (29)$$

Determining the voltage value  $U$  based on the control objective of the system by mean of minimizing the global performance index (28) at time  $k$ , in other words,  $\partial J / \partial U = 0$  and the explicit solution, we can obtain the following equation:

$$U(k) = (G^T Q G + R)^{-1} G^T Q (Z y_e(k) - F e(k) - V \tilde{X}(k) - L W(k) - H E(k)). \quad (30)$$

Thus, in each control period, the manipulated variable can obtain as follows:

$$u(k) = D (G^T Q G + R)^{-1} G^T Q (Z y_e(k) - F e(k) - V \tilde{X}(k) - L W(k) - H E(k)), \quad (31)$$

where  $D = [I \ 0 \ \dots \ 0]$ .

### 3.1.3. Stability Analysis of the Self-Adaptive Model Predictive Controller

The stability condition of the above-mentioned closed-loop of the whole system is analyzed in this section; considering the system (17), the predicted actual output at  $p$ -step can be obtained as follows:

$$y(k+P) = C_e A^P e(k) + \sum_{i=1}^P C_e A^{i-1} B u(k+P-i) + \sum_{i=1}^P C_e A^{i-1} \tilde{x}(k+P-i) + \sum_{i=1}^P C_e A^{i-1} G w(k+P-i) + \sum_{i=1}^P C_e A^{i-1} d(k+P-i). \quad (32)$$

The system (32) can be expressed under the following state-space form

$$Y(k+1) = F e(k) + G U(k) + V \tilde{X}(k) + L W(k) + V D(k), \quad (33)$$

Merging Equations (33) and (30), the predicted actual output of the closed-loop of system can be expressed as follows:

$$Y(k+1) = F e(k) + G \left( (G^T Q G + R)^{-1} G^T Q (Z y_e(k) - F e(k) - V \tilde{X}(k) - L W(k) - H E(k)) \right) + V \tilde{X}(k) + L W(k) + V D(k). \quad (34)$$

According to the performance index (26), there exists the condition depending on the weight coefficient matrix  $R$  that can limit the control input value  $U(k)$ . When it is equal to zero, the control input  $U(k)$  will be unlimited [46]. Applying this condition to Equation (34), we have:

$$Y(k+1) = Z y_e(k) - H E(k) + V D(k). \quad (35)$$

In addition, Equation (17) is calculated according to the time that is a start point ( $k - p$ ); the actual output can be obtained at time  $k$  as follows:

$$y(k) = C_e A^P e(k - P) + \sum_{i=1}^P C_e A^{i-1} B u(k - i) + \sum_{i=1}^P C_e A^{i-1} \tilde{x}(k - i) + \sum_{i=1}^P C_e A^{i-1} G w(k - i) + \sum_{i=1}^P C_e A^{i-1} d(k - i). \quad (36)$$

Combining Equations (32) and (36), and the matrix  $E(k)$  in Equation (29), we have

$$E(k) = \sum_{i=1}^P C_e A^{i-1} d(k - i) = C \tilde{D}(k), \quad (37)$$

where

$$C = \begin{bmatrix} C_e & 0 & \dots & 0 \\ C_e & C_e A & \dots & 0 \\ \vdots & \vdots & \vdots & \vdots \\ C_e & C_e A & \dots & C_e A^{P-1} \end{bmatrix} \text{ and } \tilde{D}(k) = [d(k - 1), d(k - 2), \dots, d(k - P)]^T.$$

Therefore, the actual output of the closed-loop system can be described as follows:

$$y(k + 1) = D(k) (Z y_e(k) - H C \tilde{D}(k) + V D(k)). \quad (38)$$

Equation (38) can be rewritten under another form as follows:

$$y(k + 1) = \zeta^1 y_e(k) + C_e d(k) - H_1 C_e d(k - 1). \quad (39)$$

It can be concluded that from Equation (39), the following inequality holds, if the disturbance value or its change rate is limited

$$\|C_e d(k) - H_1 C_e d(k - 1)\| \leq \xi, \quad (40)$$

so that the closed-loop control system in Equations (17) and (31) is stable, where  $\xi$  is a positive constant.

In order to prove the above conclusion is right, we decompose the system in Equation (39) into two parts as follows:

$$\begin{cases} y_1(k + 1) = \zeta^1 y_e(k), \\ y_2(k + 1) = C_e d(k) - H_1 C_e d(k - 1). \end{cases} \quad (41)$$

Obviously,  $0 < (\gamma + \tau \|e(k)\|_1) / (\mu + \|e(k)\|_1) < 1$ , thus  $\exists k_0 < \infty$  such that  $\|y_1(k + 1)\| \rightarrow 0$  when  $k > k_0$ . This given condition implies that  $\|y_2(k + 1)\| \leq \xi$ . Thus,  $\|y(k + 1)\| \leq \xi$  when  $k > k_0$ . It can be concluded that the actual status of the closed-loop control system will certainly be converged and stabilized within the neighborhood of  $\xi$ . Therefore, the closed-loop control system is constructed by the system in Equations (17) and (31) is stable.

Therefore, the steady and dynamic response capability of power follows between the DFIG-WECS, and the grid is enhanced by the proposed control scheme for RSC is as shown in Figure 3. The control signal  $u(k)$  in Equation (31) is the closed-loop system.

### 3.2. GSC Controller

The GSC is connected between the DC-link and grid via the grid filter, as shown in Figure 1. The main task is to maintain the reactive power flow between the GSC and grid at zero and the DC-link voltage at a given value. The GSC is controlled by using the inner current control loop that is used

to control the current and outer control loop that is used to control the DC-link voltage. The control strategy is implemented in the synchronously rotating  $d$ - $q$  reference frame with its  $d$ -axis oriented with the grid voltage vector based on the vector control technique that was introduced by authors in [34]. This control strategy is re-used for this study as shown in Figure 3, in which the reactive power is controlled on the remaining component  $q$  axis, whereas the  $d$  component is used to control the active power and the outer DC-link voltage loop by the PI regulators.

### 3.3. Turbine Control

In order to limit over produced power at high wind speeds and to optimize the extracted power from incoming winds, more recently, the authors in [34,48,49] have proposed the strategies to control the pitch angle. For this study, the maximum power point tracking (MPPT) model is used to control the turbine system with the pitch angle control scheme introduced by the author in [34], as shown in Figure 7. When winds are between about the cut-in speed and at a low limit speed, the reference speed of the generator rotor is set to a minimum value to ensure that the slip is smaller than 30%. When winds are between the low limit speed and the rated speed, the generator is operated in the variable speed model; the maximum power is obtained according to the reference speed that can be calculated as follows:

$$\omega_{r\_ref} = \sqrt[3]{\frac{P_m}{K_{opt}}}, \quad (42)$$

where  $K_{opt} = (1/2)(R^2/\lambda_{opt}^3)\rho\pi C_p^{max}(\beta,\lambda)$  is the optimal constant of turbine corresponding to the pitch angle equal to zero, while  $\lambda$  is adjusted to  $\lambda_{opt}$  according to different wind speeds by adapting the  $\omega_{r\_ref}$ . In addition, when winds increase larger than the rated speed, the  $\omega_{r\_ref}$  is set at the rated value, so that the over produced power is limited by adjusting the pitch angle resulting in the over speed of generator being limited.

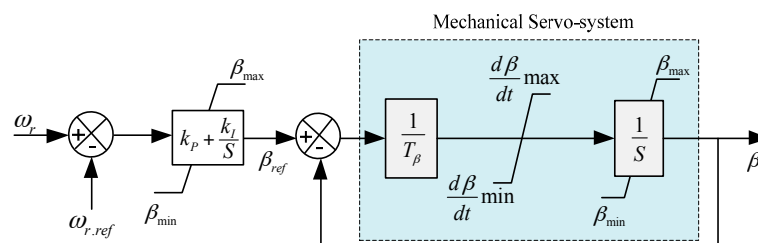


Figure 7. The pitch angle control scheme for the DFIG-WCES [34].

## 4. Case Study and Results

In order to verify the performance of the proposed method, the simulation modeling setup for the tested system including a 150 kW-575 V DFIG-WCES and 50 Hz-20 MVA/25 kV network is built in the Matlab/Simulink, as shown in Figure 6. The parameters are listed in Appendix A. In this paper, we only consider the following two scenarios:

- (i) The impact of the rotor speed variation,
- (ii) The impact of the parameter variation of the generator.

The effectiveness of the proposed control strategy is tested based on the various active and reactive power steps. Suppose that the stator active power output reference is maintained at 40% of the generator rated power, increased to 67% at 0.8 s, and then continued to increase to 100% at

1.05 s corresponding to the power factor reference value  $PF_{ref}$  of 85%,  $-85\%$ , and 100%, respectively. The reference value of the stator reactive power out can be computed according to  $PF_{ref}$  as follows

$$Q_{s.ref} = P_{s.ref} \sqrt{\frac{1}{PF_{ref}^2} - 1}. \quad (43)$$

The obtained result is compared to two difference methods that are the model predictive control introduced by authors in [31] and the discrete sliding-mode control introduced by authors in [32]. All necessary parameters of these methods are listed in the Appendix A.

#### 4.1. Case 1

The first scenario is carried out to verify the response of the system considering the variation in rotor speed. The DFIG-WSEC was operating under the speed control mode; for this study, the wind speeds were changed to from the sub-rated of 7 m/s to super-rated 15 m/s at a threshold value 0.7 s (the rated wind speed is 12 m/s), which corresponds to the increase of rotor speed from 151.2 to 172.8 rad/s at time from 0.7 s to 1.15 s, as shown in Figure 8. As known, during the period of variation wind speed, the rotor speed changes slowly since the turbine inertia is high.

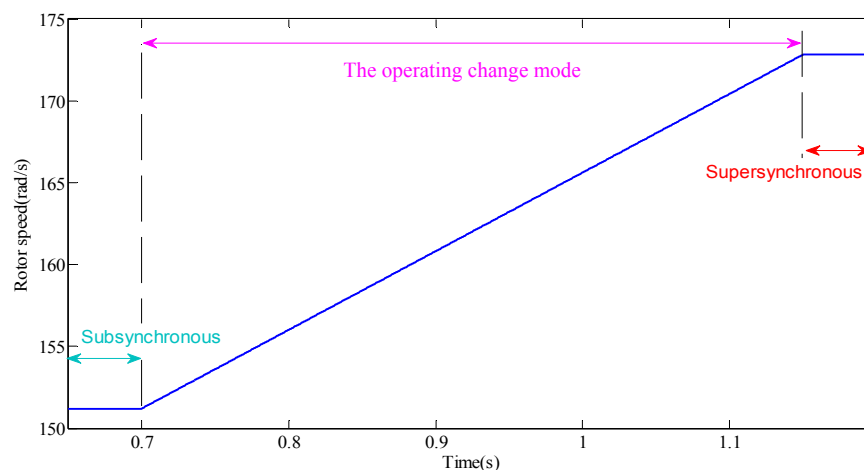
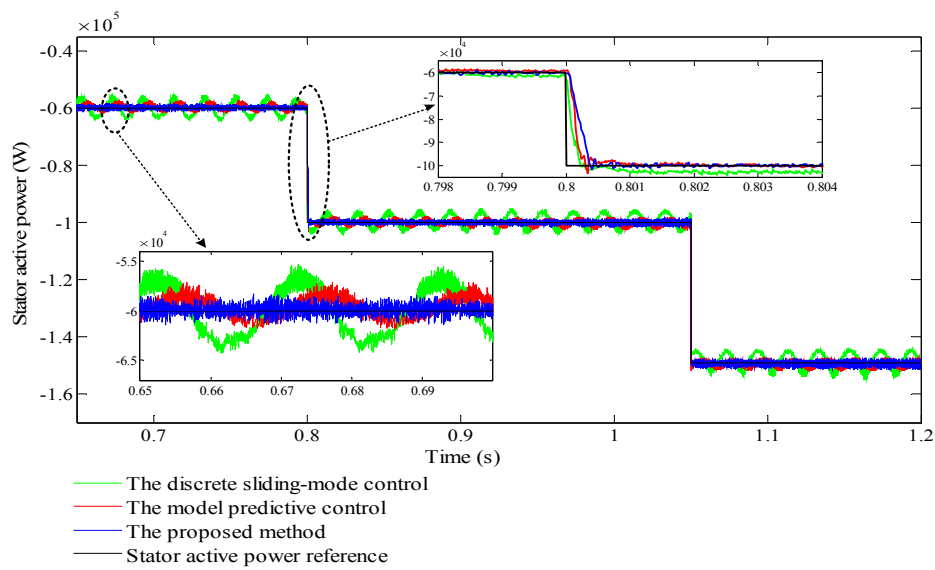


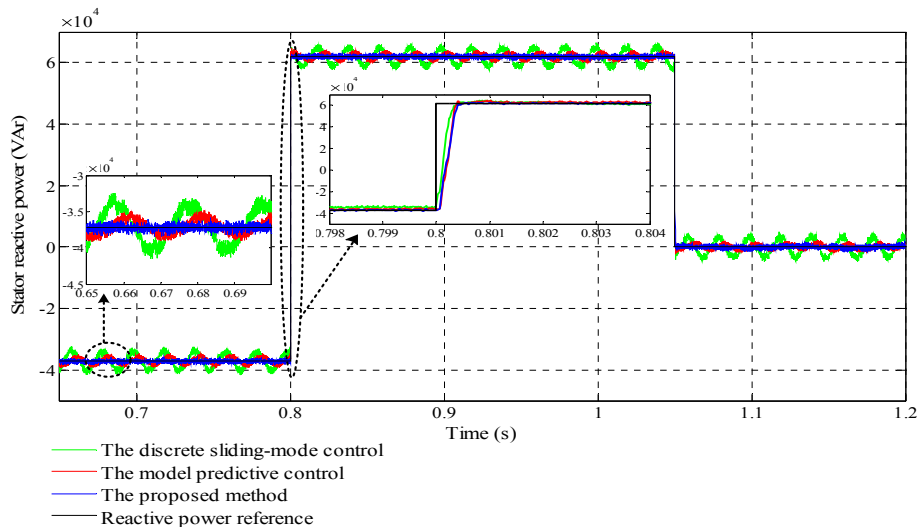
Figure 8. The rotor speed of DFIG according to the changes in wind speed.

Figure 9 plots the results of the step reference test of the stator power response, which for the steady state, a zoomed-in image of the power waveforms over period time from 0.65 to 0.69 s, the reference active power is maintained at 40% of the generator rated active power. For the transient, a zoomed-in image of the waveforms over period time from 0.798 to 0.804 s, which corresponds to the reference active power that changes the power suddenly from 40% to 67% rated power at 0.8 s. The improved steady and state-transient response characteristic can be closely observed when applying the proposed method.

Figure 10 presents the response of DC-link voltage with the given reference  $U_{ref}$  of 500 V during the steady-state and transient period. The obtained result shows that DC-link voltage oscillations have appeared as a small backward overshoot. The PI controllers of GSC, compensating the disturbances due to changing the reference active power, dampen them. It can be noticed clearly from this figure that the proposed control scheme of GSC is suitable.



(a)



(b)

**Figure 9.** Detailed steady- and transient-state response of stator power output in Case 1: (a) Active; (b) Reactive.

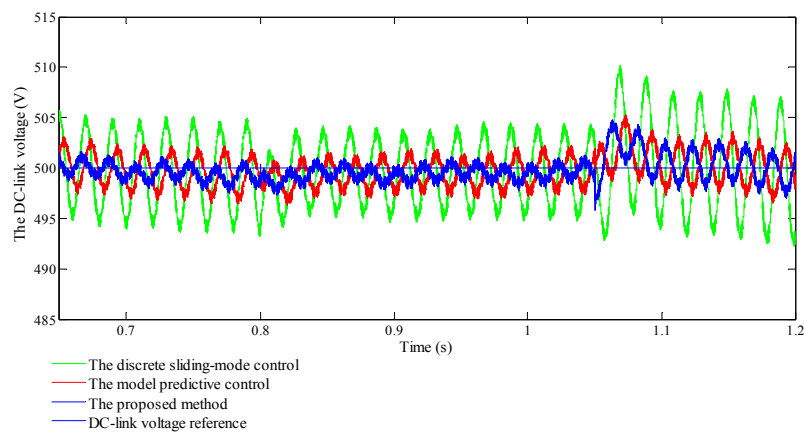


**Figure 10.** Detailed steady-state and transient response of the DC-link voltage in Case 1.

The rotor and stator three-phase currents are plotted in Figure 11. Observe from Figure 11a and two zoomed-in images of the stator current waveforms of over period time from at 0.805 to 0.825 s and from 1.025 to 1.045 s in Figure 11b that the steady-state and transient responses of currents are improved when applying the proposed method.

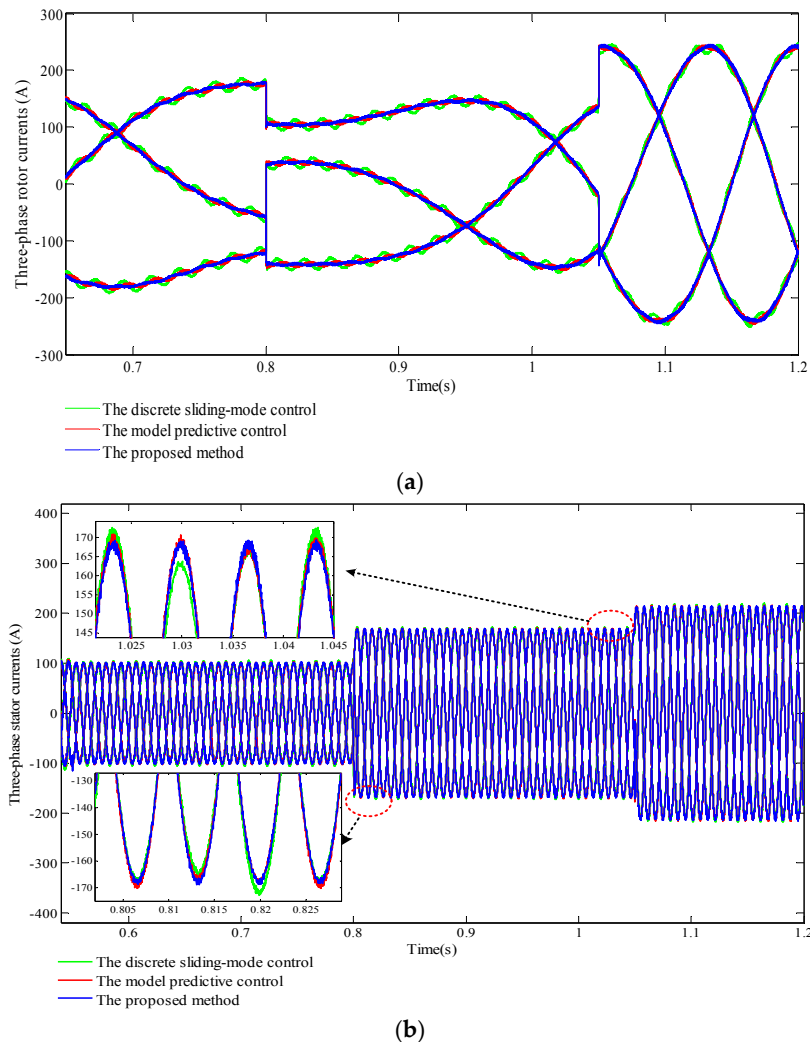


**Figure 11.** Detailed steady-state and transient response of three-phase currents in Case 1: (a) Rotor; and (b) Stator.

#### 4.2. Case 2

The second scenario is carried out to verify the effectiveness of the proposed control strategy through the same tests of step reference of active and reactive powers considering: (i) the constant rotor speed at 172.8 rad/s corresponds to the wind speed of 15 m/s and (ii) the impact of the parameter variation was introduced by increasing 20% of the nominal values of both the rotor resistance and mutual inductance parameters of the DFIG.

The result of the step reference test of stator power response is plotted in Figure 12, in which for the steady state, a zoomed-in image of the power waveforms over period time from 0.665 to 0.705 s, the reference active power is maintained at 40% of the generator rated active power. For the transient, a zoomed-in image of the power waveforms over period time from 1.04 to 1.06 s, corresponds to the reference active power that changes suddenly from 67% to 100% rated power. Figure 13 plots the detailed steady-state and transient response of the DC-link voltage and the rotor. The detailed steady-state and transient responses of three-phase currents are shown in Figure 14, in which Figure 14a

shows the oscillations of rotor currents and Figure 14b; for the steady-state, a zoomed-in image of the power waveforms over time from 0.8 to 0.83 s, the reference active power is maintained at 40% of the generator rated active power. For the transient, a zoomed-in image of the waveforms over time from 1.03 to 1.06 s, corresponding to the reference active power that suddenly changes the power from 40% to 67% rated power at 1.05 s.

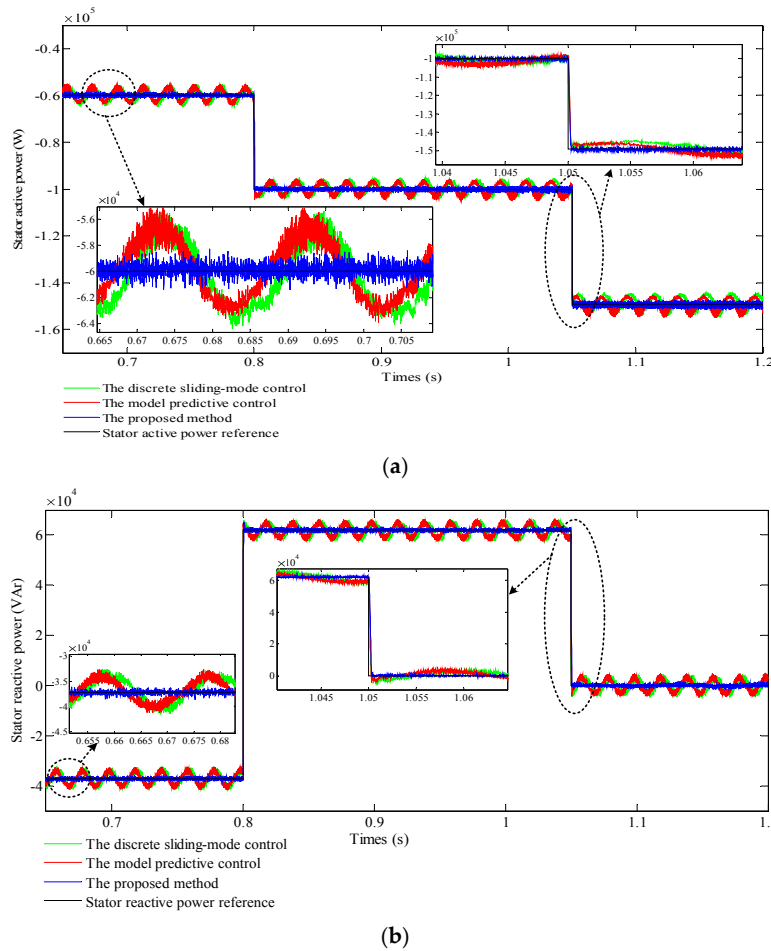


**Figure 12.** Detailed steady-state and transient response of stator power output in Case 2: (a) Active; and (b) Reactive.

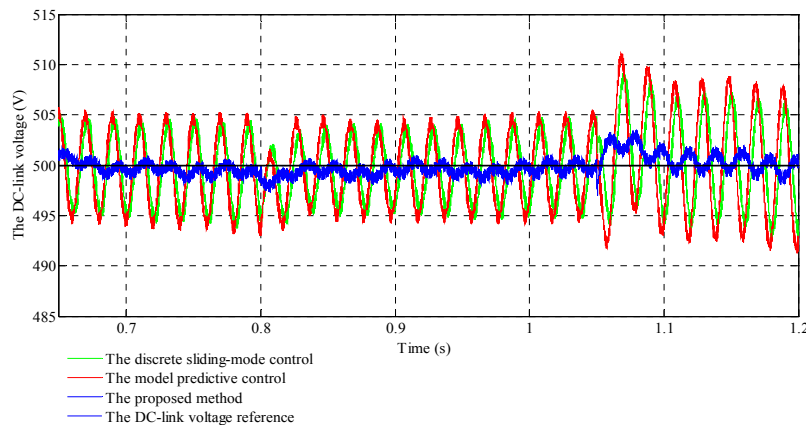


**Figure 13.** Detailed steady-state and transient response of the DC-link voltage in Case 2.

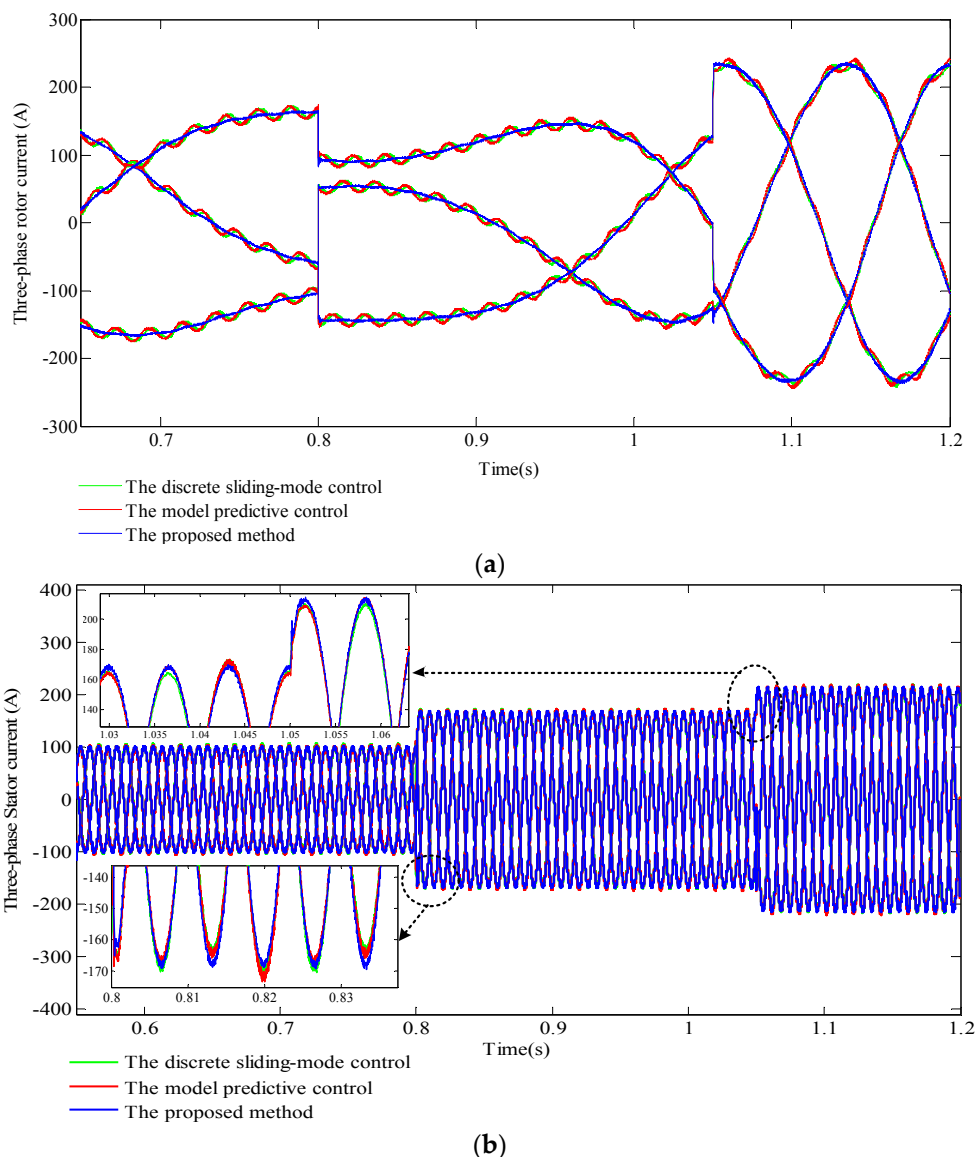


**Figure 14.** Detailed steady-state and transient response of three-phase currents in Case 2: (a) Rotor; and (b) Stator.

Comparing Figures 9 and 12, Figures 10 and 13, and Figures 11 and 14, there can difficulty in noticing any difference. Even when the variations of the rotor resistance and mutual inductance are large, the system maintains satisfactory performance under steady state and transient response.

The simulation results show that the steady state and transient responses of the active and reactive power when applying the proposed method are better than compared with two other methods, and this is because the mechanism feedback error is considered in this proposed method. In addition, it can be observed clearly that the steady-state and transient response of the stator and rotor currents are good although the proposed method does not use the current loops to control them.

### 5. Conclusions

In this paper, a feasible and efficient control strategy for the rotor converter of DFIG, making full use of properties within the generator-turbine system without using any extra, is proposed. This proposed method is developed on the model predictive control and is compared to two other methods. Based on the obtained results through the simulation of a 150 kW-575 V doubly fed induction generator

based on the wind energy converter system (DFIG-WECS) using MATLAB/Simulink, the main features of the self-adaptive model predictive control strategy are listed as follows. (i) To propose the discrete state-space model of DFIG with using the voltage oriented control mode and considering the stator power and the rotor voltage as the state and control variables is feasible and efficient, in which the stator flux was no longer explicit to avoid the error caused by flux observation; (ii) The steady-state and transient response characteristic when applying the proposed control strategy has been significantly improved compared to two conventional methods, especially when the system faces errors due to the parameter perturbations (variation of the rotor resistance and mutual inductance) and external disturbances (rotor speed verifies according to the changes of wind speed); (iii) The control of the active and reactive power does not need to use the rotor current loops. Hence, this proposed control strategy becomes a helpful power control strategy for the renewable power generation based on the WECS, and especially to DFIG.

**Acknowledgments:** The authors sincerely acknowledge the financial support provided by the National Natural Science Foundation of China (NSFC) Changsha, China under project No. 51177040.

**Author Contributions:** All the authors have contributed in the article.

**Conflicts of Interest:** The authors declare no conflict of interest.

## Nomenclature

### Symbols

$A$	State matrix of discrete state-space model
$B$	Control matrix of discrete state-space model
$C$	Output matrix of discrete state-space model
$C_e$	Output matrix of error discrete state-space model
$C_f$	Frictional coefficient
$e(.)$	State vector of error state-space model
$G$	Measurable matrix of discrete state-space model
$H_p$	Diagonal coefficient matrix
$J$	Inertia of the generator-turbine system
$K_{otp}$	Optimal constant of turbine corresponding to the pitch angle equal to zero
$L_s$	Stator inductance
$L_r$	Rotor inductance
$L_m$	Mutual inductance
$M$	Control horizon
$P$	Prediction horizon
$PF$	Power factor
$P_m$	Turbine mechanical power
$P_s$	Stator active power
$Q, R$	Pair of weight matrices in the cost function of predictive control
$Q_s$	Stator reactive power
$R$	Turbine blades radius
$R_r$	Rotor resistance
$R_s$	Stator resistance
$T_e$	Electromagnetic torque
$V_w$	Wind speed
$i_r$	Rotor current
$i_s$	Stator current
$f(k)$	External disturbances vector

$u(.)$	Input vector
$u_r$	Rotor voltage
$u_s$	Stator voltage
$w(.)$	Measurable vector
$x(.)$	State vector
$y(.)$	Output vector
$y_e(.)$	Output vector of error state-space model
$\Delta A$	State parameter perturbations matrix
$\Delta B$	Input parameter perturbations matrix
$\alpha_{i,j}$	Factors of power coefficient
$\gamma$	Tuning parameter of adjustable variable of reference trajectory
$\lambda$	Turbine tip-speed ratio
$\lambda_r$	Rotor flux
$\lambda_s$	Stator flux
$\mu$	Tuning parameter of adjustable variable of reference trajectory
$\rho$	Air density
$\sigma$	Leakage factor
$\tau$	Tuning parameter of adjustable variable of reference trajectory
$\omega_m$	Rotor mechanical angular speed
$\omega_r$	Rotor angular speed
$\omega_s$	Synchronous angular speed
$\omega_t$	Turbine rotational angular speed
$\zeta$	Adjustable variable of reference trajectory

#### Acronyms

BTB	Back-to-back
DFIG	Doubly fed induction generator
DFIG-WECS	Doubly fed induction generator based on the wind energy converter system
DPC	Direct power control
DTC	Direct torque control
GSC	Grid side converter
GWEC	Global Wind Energy Council
MPC	Model predictive control
MPPT	Maximum power point tracking
P-DPC	Predictive direct power control
PWM	Pulse width modulation
RSC	Rotor side converter
VSC	Voltage source converter
WECS	Wind energy converter system
WRIG	Wound rotor induction generator

#### Appendix A

The simulation parameters of the tested system are listed below:

- *DFIG*. Nominal power is 150 kW, voltage is 575 V, stator resistance is 0.02475  $\Omega$ , rotor resistance 0.0133  $\Omega$ , stator leakage inductance is 0.000284 H, rotor leakage inductance is 0.00284 H, mutual inductance is 0.01425 H, and inertia constant is 2.6 kg.m<sup>2</sup>.
- *Converter*. Resistance of grid filter is 0.03 p.u., inductance of grid filter is 0.3 p.u., DC-link's rated voltage is 500 V, and DC-link capacitor 0.01 F.
- *GSC control*. The DC-link voltage regulator:  $K_p = 112.4$ ,  $K_i = 25.6$ ; the current power regulator ( $d$ -axis):  $K_p = 9.7$ ,  $K_i = 0.04$ ; the current power regulator ( $q$ -axis):  $K_p = 9.7$ ,  $K_i = 0.04$ .
- *The pitch angle controller*.  $K_p = 100$ ,  $K_i = 8$ ,  $\beta_{max} = 45$  degrees,  $\beta_{min} = 0$  degrees,  $T_\beta = 0.1$  s.
- *Other Parameters of Per Control method*.

**Table A1.** Other parameters of per control method.

Parameters	Methods		
	Proposed	Model Predictive	Sliding-Mode
	Value		
The control period	$T_c = 5 \times 10^{-5}\text{s}$	$T_c = 5 \times 10^{-5}\text{s}$	$T_c = 5 \times 10^{-5}\text{s}$
The weighting matrices	$Q = \begin{bmatrix} 10 & 0 \\ 0 & 1 \end{bmatrix}$ $R = \begin{bmatrix} 25 & 0 \\ 0 & 15 \end{bmatrix}$	$Q = \begin{bmatrix} 10 & 0 \\ 0 & 1 \end{bmatrix}$ $R = \begin{bmatrix} 25 & 0 \\ 0 & 15 \end{bmatrix}$	-
The prediction P and control horizon M	P = 2 M = 1	P = 2 M = 1	-
The first and second coefficient diagonal matrices	$H_1 = \begin{bmatrix} 0.90 & 0 \\ 0 & 0.90 \end{bmatrix}$ $H_2 = \begin{bmatrix} 0.45 & 0 \\ 0 & 0.45 \end{bmatrix}$	-	-
The output matrix	$C = \begin{bmatrix} 1 & 0 \\ 0 & 1 \end{bmatrix}$	$C = \begin{bmatrix} 1 & 0 \\ 0 & 1 \end{bmatrix}$	$C = \begin{bmatrix} 1 & 0 \\ 0 & 1 \end{bmatrix}$
Another condition constant	$\mu = 1000, \gamma = 700,$ and $\tau = 0.3$	-	$\varepsilon T_c = 0.1,$ and $\delta T_c = 0.6$

## References

1. The Global Wind Report Annual Market Update 2015. Available online: <http://www.gwec.net> (accessed on 25 April 2016).
2. Soliman, M.; Malik, O.P.; Westwick, D.T. Multiple model predictive control for wind turbines with doubly fed induction generators. *IEEE Trans. Sustain. Energy* **2011**, *2*, 215–225. [CrossRef]
3. Vinothkumar, K.; Selvan, M.P. Novel scheme for enhancement of fault ride-through capability of doubly fed induction generator based wind farms. *Energy Convers. Manag.* **2011**, *52*, 2651–2658. [CrossRef]
4. Muller, S.; Deicke, M.; De Doncker, R.W. Doubly fed induction generator systems for wind turbines. *IEEE Ind. Appl. Mag.* **2002**, *8*, 26–33. [CrossRef]
5. Abad, G.; Lopez, J.; Rodríguez, M.; Marroyo, L.; Iwanski, G. *Doubly Fed Induction Machine: Modeling and Control for Wind Energy Generation*; John Wiley & Sons: Hoboken, NJ, USA, 2011.
6. Petru, T.; Thiringer, T. Modeling of wind turbines for power system studies. *IEEE Trans. Power Syst.* **2002**, *17*, 1132–1139. [CrossRef]
7. Qiao, W.; Harley, W.; Venayagamoorthy, G.K. Dynamic modeling of wind farms with fixed-speed wind turbine generators. In Proceedings of the 2007 IEEE Power Engineering Society General Meeting, Tampa, FL, USA, 24–28 June 2007; pp. 1–8.
8. Ackermann, T. *Wind Power in Power Systems*; John Wiley & Sons: Hoboken, NJ, USA, 2005.
9. Hu, J.; He, Y.; Xu, L.; Williams, B.W. Improved control of DFIG systems during network unbalance using PI-R current regulators. *IEEE Trans. Ind. Electron.* **2009**, *56*, 439–451. [CrossRef]
10. Chondrogiannis, S.; Barnes, M. Stability of doubly-fed induction generator under stator voltage orientated vector control. *IET Renew. Power Gener.* **2008**, *2*, 170–180. [CrossRef]
11. Hao, S.; Abdi, E.; Barati, F.; McMahon, R. Stator-flux-oriented vector control for brushless doubly fed induction generator. *IEEE Trans. Ind. Electron.* **2009**, *56*, 4220–4228.
12. Hopfensperger, B.; Atkinson, D.J.; Lakin, R.A. Stator-flux-oriented control of a doubly-fed induction machine with and without position encoder. *IEE Proc. Electr. Power Appl.* **2000**, *147*, 241–250. [CrossRef]
13. Pena, R.; Clare, J.C.; Asher, G.M. Doubly fed induction generator using back-to-back PWM converters and its application to variable-speed wind-energy generation. *IEE Proc. Electr. Power Appl.* **1996**, *143*, 231–241. [CrossRef]
14. Zhi, D.; Xu, L. Direct power control of DFIG with constant switching frequency and improved transient performance. *IEEE Trans. Energy Convers.* **2007**, *22*, 110–118. [CrossRef]

15. Takahashi, I.; Noguchi, T. A new quick-response and high-efficiency control strategy of an induction motor. *IEEE Trans. Ind. Appl.* **1986**, *22*, 820–827. [[CrossRef](#)]
16. Depenbrock, M. Direct self-control (DSC) of inverter-fed induction machine. *IEEE Trans. Power Electron.* **1988**, *3*, 420–429. [[CrossRef](#)]
17. Baader, U.; Depenbrock, M.; Gierse, G. Direct self control (DSC) of inverter-fed induction machine: A basis for speed control without speed measurement. *IEEE Trans. Ind. Appl.* **1992**, *28*, 581–588. [[CrossRef](#)]
18. Kazmierkowski, M.P.; Kasprowicz, A.B. Improved direct torque and flux vector control of PWM inverter-fed induction motor drives. *IEEE Trans. Ind. Electron.* **1995**, *42*, 344–350. [[CrossRef](#)]
19. Vas, P. *Sensorless Vector and Direct Torque Control*; Oxford University Press: Oxford, UK, 1998.
20. Buja, G.S.; Kazmierkowski, M.P. Direct torque control of PWM inverter-fed AC motors—A survey. *IEEE Trans. Ind. Electron.* **2004**, *51*, 744–757. [[CrossRef](#)]
21. Datta, R.; Ranganathan, V.T. Direct power control of grid-connected wound rotor induction machine without rotor position sensors. *IEEE Trans. Power Electron.* **2001**, *16*, 390–399. [[CrossRef](#)]
22. Xu, L.; Cartwright, P. Direct active and reactive power control of DFIG for wind energy generation. *IEEE Trans. Energy Convers.* **2006**, *21*, 750–758. [[CrossRef](#)]
23. Mohd Zin, A.A.B.; Mahmoud Pesaran, H.A.; Khairuddin, A.B.; Jahanshaloo, L.; Shariati, O. An overview on doubly fed induction generators' controls and contributions to wind based electricity generation. *Renew. Sustain. Energy Rev.* **2013**, *27*, 692–708. [[CrossRef](#)]
24. Zhi, D.; Xu, L.; Williams, B.W. Model-based predictive direct power control of doubly fed induction generators. *IEEE Trans. Power Electron.* **2010**, *25*, 341–351.
25. Hu, J.; Zhu, J.; Dorrell, D.G. Model-predictive direct power control of doubly-fed induction generators under unbalanced grid voltage conditions in wind energy applications. *IET Renew. Power Gener.* **2014**, *8*, 687–695. [[CrossRef](#)]
26. Abad, G.; Rodríguez, M.Á.; Poza, J. Three-level NPC converter-based predictive direct power control of the doubly fed induction machine at low constant switching frequency. *IEEE Trans. Ind. Electron.* **2008**, *55*, 4417–4429. [[CrossRef](#)]
27. Cortés, P.; Kazmierkowski, M.P.; Kennel, R.M.; Quevedo, D.E.; Rodríguez, J. Predictive control in power electronics and drives. *IEEE Trans. Ind. Electron.* **2008**, *55*, 4312–4324. [[CrossRef](#)]
28. Rodríguez, J.; Cortes, P. *Predictive Control of Power Converters and Electrical Drives*; John Wiley & Sons: Hoboken, NJ, USA, 2012; Volume 40.
29. Wang, X.; Sun, D. Three-Vector-Based Low-Complexity Model Predictive Direct Power Control Strategy for Doubly Fed Induction Generators. *IEEE Trans. Power Electron.* **2017**, *32*, 773–782. [[CrossRef](#)]
30. ALarrinaga, S.; Vidal, M.A.R.; Oyarbide, E.; Apraiz, J.R.T. Predictive control strategy for DC/AC converters based on direct power control. *IEEE Trans. Ind. Electron.* **2012**, *54*, 1261–1271. [[CrossRef](#)]
31. Sguarezi Filho, A.J.; Ruppert Filho, E. Model-based predictive control applied to the doubly-fed induction generator direct power control. *IEEE Trans. Sustain. Energy* **2012**, *3*, 398–406. [[CrossRef](#)]
32. Hu, J.; Nian, H.; Hu, B.; He, Y.; Zhu, Z.Q. Direct active and reactive power regulation of DFIG using sliding-mode control approach. *IEEE Trans. Energy Convers.* **2010**, *25*, 1028–1039. [[CrossRef](#)]
33. Shang, L.; Hu, J. Sliding-mode-based direct power control of grid-connected wind-turbine-driven doubly fed induction generators under unbalanced grid voltage conditions. *IEEE Trans. Energy Convers.* **2012**, *27*, 362–373. [[CrossRef](#)]
34. Le, V.; Li, X.; Li, Y.; Dong, T.L.T.; Le, C. An Innovative Control Strategy to Improve the Fault Ride-Through Capability of DFIGs Based on Wind Energy Conversion Systems. *Energies* **2016**, *9*, 69. [[CrossRef](#)]
35. Iov, F.; Hansen, A.D.; Sorensen, P.; Blaabjerg, F. *Wind Turbine Blockset in Matlab/Simulink*; Aalborg University: Aalborg, Denmark, 2004.
36. Miller, N.W.; Price, W.W.; Sanchez-Gasca, J.J. *Dynamic Modeling of GE 1.5 and 3.6 Wind Turbine-Generators*; GE—International, Power Systems Energy Consulting: Schenectady, NY, USA, 2003.
37. Tohidi, A.; Abedinia, O.; Bekravi, M.; Ojaroudi, N. Multivariable adaptive variable structure disturbance rejection control for DFIG system. *Complexity* **2014**. [[CrossRef](#)]
38. Wu, B.; Lang, Y.; Zargari, N.; Kouro, S. *Power Conversion and Control of Wind Energy System*; John Wiley & Sons: Hoboken, NJ, USA, 2011.
39. Hindmarsh, J. *Worked Examples in Electrical Machines and Drives: Applied Electricity and Electronics*; Elsevier: Amsterdam, The Netherlands, 1982.

40. Yamamura, S. *Spiral Vector Theory of AC Circuits and Machines*; Oxford University Press: Oxford, UK, 1992.
41. Holtz, J.; Quan, J.; Pontt, J.; Rodríguez, J.; Newman, P.; Miranda, H. Design of fast and robust current regulators for high-power drives based on complex state variables. *IEEE Trans. Ind. Appl.* **2004**, *40*, 1388–1397. [[CrossRef](#)]
42. Franklin, G.F.; Powell, J.D.; Workman, M.L. *Digital Control of Dynamic Systems*; Addison-Wesley: Boston, MA, USA, 1998; Volume 3.
43. Perruquetti, W.; Barbot, J.P. *Sliding Mode Control in Engineering*; CRC Press: Beijing, China, 2002.
44. Seborg, D.E.; Mellichamp, D.A.; Edgar, T.F.; Doyle, F.J., III. *Process Dynamics and Control*; John Wiley & Sons: Hoboken, NJ, USA, 2010.
45. Li, S.; Zheng, Y. *Distributed Model Predictive Control for Plant-Wide Systems*; John Wiley & Sons: Hoboken, NJ, USA, 2016.
46. Xi, Y.G. *Predictive Control*; PRC Press: Beijing, China, 1993.
47. Maciejowski, J.M. *Predictive Control with Constraints*; Prentice-Hall: Harlow, UK, 2002.
48. Duong, M.Q.; Grimaccia, F.; Leva, S.; Mussetta, M.; Ogliari, E. Pitch angle control using hybrid controller for all operating regions of SCIG wind turbine system. *Renew. Energy* **2014**, *70*, 197–203. [[CrossRef](#)]
49. Duong, M.Q.; Grimaccia, F.; Leva, S.; Mussetta, M.; Le, K.H. Improving transient stability in a grid-connected squirrel-cage induction generator wind turbine system using a fuzzy logic controller. *Energies* **2015**, *8*, 6328–6349. [[CrossRef](#)]



© 2017 by the authors. Licensee MDPI, Basel, Switzerland. This article is an open access article distributed under the terms and conditions of the Creative Commons Attribution (CC BY) license (<http://creativecommons.org/licenses/by/4.0/>).